INTERNATIONAL JOURNAL of RENEWABLE ENERGY RESEARCH
O. Echab et al., Vol.16, No.2, June, 2026

A Nonlinear Backstepping Controller for Grid Connected Photovoltaic System

Oumaima Echab *‡, Noureddine Ech-Cherki, Abdellatif Obbadi *, Youssef Errami*, Smail Sahnoun*, Mohssin Aoutoul*

*Laboratory: Electronics, Instrumentation and Energy (LEIE), Faculty of Science, Chouaib Doukkali University, Route Ben Maachou, 24000 El Jadida, Morocco

(echab.o@ucd.ac.ma, cherki.ucd@gmail.com, obbadi.a@ucd.ac.ma, errami.y@ucd.ac.ma, sahnoun.s@ucd.ac.ma, aoutoul.m@ucd.ac.ma)

‡Corresponding Author; Oumaima ECHAB, Laboratory: Electronics, Instrumentation and Energy(LEIE), Faculty of Science, Chouaib Doukkali University, Route Ben Maachou, 24000 El Jadida, Morocco, Tel: +212 641134754, echab.o@ucd.ac.ma

Received: 23.02.2024 Accepted: 08.04.2024

Abstract- This paper presents a nonlinear backstepping control design for a grid connected Photovoltaic (PV) system. This controller is used for a DC-DC boost converter to control the output voltage of the PV array according to a reference voltage produced by the Incremental Conductance (IC) algorithm. It is also applied to control the three phase inverter grid side to manage the DC bus voltage, active and reactive powers. The proposed controller is based on Lyapunov function to ensure the stability and to increase the effectiveness of the PV system. Simulation results are obtained in a Matlab/Simulink environment. The results indicate an excellent rapid response and fewer fluctuations even under the varying environmental conditions. It offers also an optimal PV power and a significant quality of current injected into the grid. Furthermore, it confirms the robustness in terms of injecting maximum active power into the grid, while keeping the DC bus voltage and the reactive power fixed at certain values. The validity of the Backstepping Controller (BSC) is proved with regard to extracting the Maximum Power Point (MPP) which is compared to the classic IC algorithm. Moreover, it is also demonstrated in the matter of controlling the Pulse Width Modulation (PWM) of the three phase inverter in comparison to the classic Proportional Integral (PI) controller.

Keywords Backstepping control, grid connected PV system, incremental conductance algorithm, lyapunov function, MPPT, PI controller.

Nomenclature list

μ	Duty cycle	P_a	Active power (W)
A	Diode ideality factor of PV cell	P_{pv}	PV array power (W)
C_{dc}	Output capacitor (F)	q	Charge of electron (=1.602*10^{-19}C)
C_{pv}	Input capacitor (F)	Q	Reactive power (VAR)
D	Diode of boost converter	Q_{ref}	Reference of reactive power (VAR)
I	Output current of PV cell (A)	R_f	Resistance of three phase filter (Ω)
I_{Cdc}	Current of output capacitor (A)	R_s	Series resistance of PV cell and PV array (Ω)
I_{Cpv}	Current of input capacitor (A)	R_{sh}	Parallel resistance of PV cell and PV array (Ω)

i_{dg}	Direct current of the inverter output (A)	T	Switch of boost converter
i_g	Input current of the inverter (A)	T	Temperature (°K)
I_L	Current of the inductor of boost converter (A)	V	Output voltage of PV cell (V)
I_{ph}	Photocurrent of the PV cell (A)	V_{dc}	Voltage of output capacitor (V)
i_{pv}	Output current of the PV array (A)	V_{dcref}	Reference of voltage of output capacitor (V)
i_{qg}	Quadrature current of the inverter output (A)	V_{iabc}	inverter voltages (V)
I_s	Diode reverse saturation current of PV cell (A)	V_{gabc}	Grid voltages (V)
GPV	Group of photovoltaic panels	V_{gd}	Direct voltage of the inverter output (V)
K	Boltzmann's constant (=1.3806*10^{-23} J/K)	V_{mpp}	Voltage of module at maximum power point (V)
L	Inductor of boost converter (H)	V_{pv}	Output voltage of PV array (V)
L_f	Inductor of three phase filter (H)	V_{pvref}	Reference voltage of PV voltage (V)
N_{pp}	Number of PV panels connected in parallel	V_{qg}	Quadrature voltage of the inverter output (V)
N_s	Number of cells per module	V_t	Thermal voltage (V)
N_{ss}	Number of PV panels connected in series	ω	Pulsation of grid (rad/s)

1. Introduction

Renewable energy has come more popular in current years because of the fact that it is sustainable and environmentally friendly [1], ease of installation, and low maintenance requirements. Photovoltaic (PV) energy is the most important renewable energy technology. The PV system can operate in two modes, standalone mode [2] and grid connected mode [3]. The first mode is used for low power applications and it demands a battery bank for the energy storage. While, the grid connected mode is used for high power applications. The energy transmission process is passing by a couple of steps that's lead finally to inject this energy coming from the PV array into the grid. The output power of the PV generator varies with environmental conditions [4]. Therefore, the PV array shows a nonlinear voltage-current characteristic, and it delivers the maximum power at the Maximum Power Point (MPP). A plenty of attainments have been created at this moment, on the Maximum Power Point Tracking (MPPT) algorithms of PV power generations. The classic ones like Perturb and Observe (P&O) and incremental conductance (IC) [5-8] are the mostly used thanks to their cheap cost and easy implementation. Those types of tracking methods are capable to pursue the MPP while the environmental conditions stay consistent. Moreover, the classic MPPT algorithms pose many drawbacks, such as high oscillations near the MPP that conduce to power losses [9]. Furthermore, they have a lower converging speed and adrift issues linked to the fast change in irradiation [10]. The injection of PV power into the grid also requires a grid side control, which consists of controlling the Pulse Width Modulation (PWM) of a three phase inverter by managing the maximum active power and fixing the values of DC bus voltage and the reactive power. In this respect, several realizations have been implemented. The classic Proportional Integral (PI) controller is commonly employed in literature [11] due to its affordability, durability and ease of implementation. Even if it shows good performances, but this controller has a set of problems tacking for example the high converging delay.

By reason of the aforementioned limitations, researchers all over the world are developing novel and different controlling techniques utilizing PV systems, in seek of obtaining a better achievement and high performances, a various nonlinear control techniques have been applied. Among these techniques we can find the Backstepping Controller (BSC), which is a nonlinear technique utilized to get rid of the complexity of the nonlinear systems. Z. El Idrissi [12] have applied the BSC to control a DC-DC converter type Buck-Boost. In addition, Naghmash et al [13] have used the BSC for the non-inverted buck-boost converter. Furthermore, T. K. Roy and M. A. Mahmud [14], have established the BSC for AC/DC micro grid. In all the preceding works, the authors have verified and approved that the BSC has an excellent performance for controlling different PV systems. Contrary to the studies of [12- 14], our work suggests an entire study of the BSC for regulating the PV chain to control both the MPPT and the inverter grid sides, duo to reducing oscillations and ameliorating efficiency during variable environmental conditions. In the first place, the BSC is used to control the duty cycle of a DC-DC boost converter. A reference voltage

of the PV array is produced by an IC algorithm, which utilized to control the output voltage of the PV array to finally reach the MPP rapidly. In the second place, the BSC is employed to regulate the active power delivered from the PV array to the grid by controlling the DC bus voltage and maintaining the reactive power at a fixed values. The essential objective of this work is to confirm the effectiveness and the validity of the BSC during various environmental conditions. Likewise, two comparative analysis are made. The first one between the classic IC and the IC-Backstepping Controller (IC-BSC) algorithms at the MPPT level, and the second was made between the BSC and PI controller on the inverter grid side. This paper can assist other researchers and engineers in enhancing and improving their research by offering a rapid response with minimal loss, which enhances the efficiency of the PV system.

The current paper is organized as follows, the PV system presentation and its modeling is shown in section 2. The BSC steps design is presented in section 3, which is divided into two parts. The first one is dedicated to the MPPT side control, while the second is dedicated to the inverter grid side control. The results of this technique and its comparisons are exposed in section 4, and finally the conclusion is given in the final section 5.

2. Presentation and Modeling of PV System

The structure of the PV system is given in Fig. 1. The configuration of this system contains a PV array that produces electrical energy based on environmental change, a DC-DC boost converter and an inverter connected to the grid, which are controlled by the backstepping technique. The IC algorithm produces a reference voltage Vpvref, which is regulated by the BSC in the reason of generating a nonlinear control duty cycle μ that adjusts the pulse width signal of the DC-DC boost converter. The grid generates a three phase voltage and current that are transformed into dq plan via Park transformation, into the object of controlling the DC bus voltage Vdc, the active and the reactive powers using the BSC.

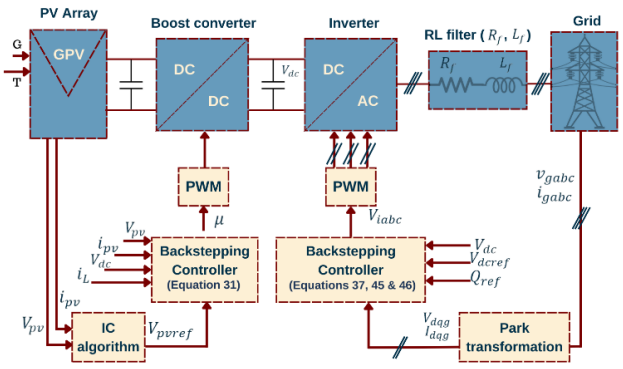

Fig. 1. Photovoltaic system structure.

The selected PV panel in this paper is multicrystalline KC200GT [15]. The present study employs the single diode model. The five parameters of the cell are estimated by using the iterative method as described in [15]. The equivalent model of a PV panel is represented as a PV cell [16]. As shown in Fig. 2, at the same environmental conditions for all the cells. The principal model parameters contain the photocurrent Iph, the diode reverse saturation current I_s, diode ideality factor A, series resistance R_s, and the parallel resistance R_{sh}. The characteristic equation of a PV module [16] is presented by:

$$I = I_{ph} - I_s\left[\exp\left(\frac{V + R_s.I}{A.N_S.V_t}\right) - 1\right] - \frac{V + R_s.I}{R_{sh}} \quad (1)$$

The PV array model can be expressed as:

$$I = N_{pp}.I_{ph} - N_{pp}.I_s\left[\exp\left(\frac{N_{ss}.V + R_s.I\left(\frac{N_{ss}}{N_{pp}}\right)}{A.N_s.V_t.N_{ss}}\right) - 1\right] - \left(\frac{N_{ss}.V + R_s.I\left(\frac{N_{ss}}{N_{pp}}\right)}{R_{sh}\left(\frac{N_{ss}}{N_{pp}}\right)}\right) \quad (2)$$

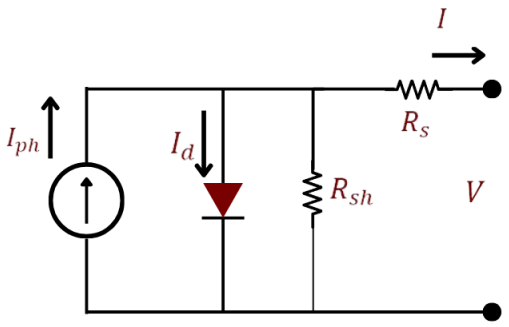

Fig. 2. Equivalent model of photovoltaic modüle.

The first stage of the PV system is a DC-DC boost converter, which is used to increase a DC voltage to reach the voltage Vmpp of the PV array at the maximum power point by modifying the value of duty cycle μ. In the current work, the DC-DC boost converter is operating in Continuous Conductance Mode (CCM), which the converter operates in two states. State ON, when the switch T is conducting and the diode D is not. State OFF is the second state of switching when the diode D is conducting while the switch T is not. The dynamic models of the two operating modes are obtained by applying Kirchhoff's laws [17].

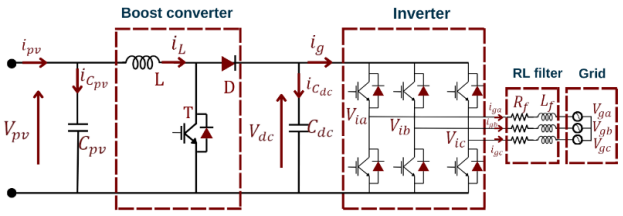

Fig. 3. Electrical model of the PV system.

According to Fig. 3, the two models of state ON and state OFF of the DC-DC boost converter are described as:

- State ON (at the period μTs), using Kirchhoff's laws, we find:

$$\begin{cases} i_{c_{pv}} = C_{pv}\dfrac{dV_{pv}}{dt} = i_{pv} - i_L \\ i_{c_{dc}} = C_{dc}\dfrac{dV_{dc}}{dt} = -i_g \\ V_L = L\dfrac{di_L}{dt} = V_{pv} \end{cases} \quad (3)$$

- State OFF (at the period (1-μ)Ts), with Kirchhoff's laws, we get:

$$\begin{cases} i_{c_{pv}} = C_{pv}\dfrac{dV_{pv}}{dt} = i_{pv} - i_L \\ i_{c_{dc}} = C_{dc}\dfrac{dV_{dc}}{dt} = i_L - i_g \\ V_L = L\dfrac{di_L}{dt} = V_{pv} - V_{dc} \end{cases} \quad (4)$$

The following averaging expression is commonly used to identify a dynamic representation that is logical for the entire period Ts [17].

$$\frac{dx}{dt}Ts = \frac{dx}{dt_{\mu Ts}}\mu Ts + \frac{dx}{dt_{(1-t)Ts}}(1-\mu)Ts \quad (5)$$

Obtaining the state-space average model [17] of the DC-DC boost converter is achieved by replacing the Eq.5 into the equations 3 and 4, which yield to:

$$\begin{cases} \dfrac{dV_{pv}}{dt} = \dfrac{1}{C_{pv}}\left(i_{pv} - i_L\right) \\ \dfrac{dV_{dc}}{dt} = (1-\mu)\dfrac{i_L}{C_{dc}} - \dfrac{i_g}{C_{dc}} \\ \dfrac{di_L}{dt} = \dfrac{1}{L}\left(V_{pv} - (1-\mu)V_{dc}\right) \end{cases} \quad (6)$$

$$\begin{cases} \dot{x}_1 = \dfrac{1}{C_{pv}}\left(i_{pv} - x_2\right) \\ \dot{x}_2 = \dfrac{1}{L}\left(x_1 - (1-\mu)V_{dc}\right) \end{cases} \quad (7)$$

Where the average state vector is $x = [x_1\ x_2]^T = [V_{pv}\ i_L]^T$ and the duty cycle is μ (0<μ<1).

The second stage of the PV system is an inverter that generates a three phase current injected into the grid. The link between the inverter and the grid is made by a three phase RL filter. Using park transformation [18], the direct and the quadrature voltage of the inverter output are given as:

$$v_{dg} = v_{di} - R_f i_{dg} - L_f\frac{di_{dg}}{dt} + \omega L_f i_{qg} \quad (8)$$

$$v_{qg} = v_{qi} - R_f i_{qg} - L_f\frac{di_{qg}}{dt} - \omega L_f i_{dg} \quad (9)$$

The active and reactive power outputs can be presented as [11]:

$$P_a = \frac{3}{2}v_{dg}i_{dg} \quad (10)$$

$$Q = -\frac{3}{2}v_{dg}i_{qg} \quad (11)$$

Corresponding to Fig. 3, the power of the V_{dc} is presented by:

$$\frac{1}{2}C_{dc}\frac{dV^2_{dc}}{dt} = P_{out} - P_a \quad (12)$$

From Eq. (12), it is obvious that the P_{out} acts as a disturbance, and the V_{dc} provides the active grid power reference value P_{gref}. Eq. (12) leads to a nonlinear system with respect to V_{dc}.

The nonlinear system is obtained, by combining Equations from (8) to (12). The system is described as:

$$\frac{di_{dg}}{dt} = -\lambda_1 i_{dg} + \lambda_2 i_{qg} + \lambda_3\left(v_{di} - v_{dg}\right) \quad (13)$$

$$\frac{di_{qg}}{dt} = -\lambda_1 i_{qg} - \lambda_2 i_{dg} + \lambda_3 v_{qi} \quad (14)$$

$$\frac{dV_{dc}}{dt} = \frac{2}{C_{dc}}\left(-\frac{3}{2}v_{dg}i_{dg} + P_{out}\right) \quad (15)$$

Where $\lambda_1 = R_f/L_f$, $\lambda_2 = \omega$ and $\lambda_3 = 1/L_f$

3. Backstepping Controller Steps

3.1. MPPT Side Control

IC algorithm is based on the knowledge of the changes in PV module conductance and their consequences on the location of the operating point in relation to an MPP. The purpose is to track the V_{pv} to V_{pvref} produced from the IC algorithm which is presented in Fig. 4. This algorithm is utilized to extract the maximum Vpvref in order to elaborate the Backstepping MPPT. The IC algorithm [19] is introduced in Fig. 4. By regulating the duty cycle μ of the DC-DC boost converter, the objective of the BSC in this step is to track the Vpv towards the Vmpp for the sake of extracting the maximum power from the PV array. For this purpose, firstly the error signal is defined as [13]:

$$\varepsilon_1 = V_{PV} - V_{pvref} \quad (16)$$

The desired result can be obtained by converging ε_1 to zero. The derivative of Eq. (16) is obtained as:

$$C_{pv} \qquad (17)$$

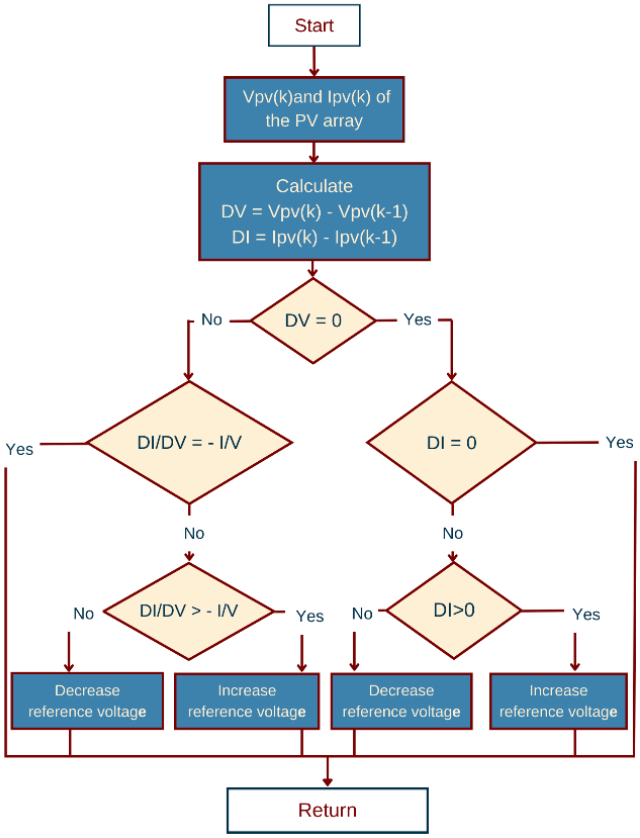

Fig. 4. Flow chart of IC algorithm.

To guarantee the asymptotic stability and the attractiveness conditions, one of the basic Lyapunov functions is chosen, it is given by:

$$V_1 = \frac{1}{2}\varepsilon_1^{\,2} \qquad (18)$$

The derivative of Eq (18) is presented as follows:

$$\left[C_{pv} \right] \qquad (19)$$

For the sake of maintaining the asymptotic stability, V_1 should be positive while its derivative needs to be negative

With:

$$-\beta_1\varepsilon_1 = \frac{1}{C_{pv}}\left(i_{pv} - x_2\right) - \qquad (20)$$

Where:

$$x_2 = C_{pv}\left(\beta_1\varepsilon_1 - \right) \qquad (21)$$

Replacing (21) in (19), the Eq. (19) becomes:

$$\qquad (22)$$

Since the derivative of V_1 is definitely negative, the value of β_1 is a positive design parameter ($\beta_1>0$).

The stabilization function is given by:

$$\alpha = C_{pv}\left(\beta_1\varepsilon_1 - \right) \qquad (23)$$

Which α acts as the current reference of x_2

In favor of tracking x_2 to its reference α, an error ε_2 is presented as:

$$\varepsilon_2 = x_2 - \alpha \qquad (24)$$

With:

$$x_2 = \varepsilon_2 + \alpha \qquad (25)$$

Differentiating Eq. (25), Eq. (17) becomes:

$$\frac{1}{C_{pv}}\left(\alpha + \varepsilon_2\right) + \frac{1}{C_{pv}} i_{pv} - \qquad (26)$$

The derivative of Eq. (24), can be presented as:

$$L \qquad (27)$$

A composite Lyapunov function V_2 is represented for providing the asymptotic stability and to make the errors ε_1 and ε_2 converge to zero. It is necessary for V_2's derivative to be negative.

$$V_2 = V_1 + \frac{1}{2}\varepsilon_2^{\,2} \qquad (28)$$

Differentiating Eq. (28), therefore:

$$+\varepsilon_2\left[-\frac{1}{C_{pv}}\varepsilon_1 + \frac{1}{L}\left(V_{pv} - (1-\mu)V_{dc}\right) - \right] \qquad (29)$$

The derivative of V_2 is definitively negative, then:

$$\left(-\frac{1}{C_{pv}}\varepsilon_1 + \frac{1}{L}\left(V_{pv} - (1-\mu)V_{dc}\right) - \right) \qquad (30)$$

For that reason, the μ command is expressed by:

$$\mu = 1 - \frac{1}{V_{dc}}\left[V_{pv} - L\dot{\alpha} - L\left(\frac{1}{C_{pv}}\varepsilon_1 - \beta_2\varepsilon_2\right)\right] \qquad (31)$$

With β_2 is a positive design parameter ($\beta_2>0$), that's lead to the negative derivative of Lyapunov function. Which guarantees the convergence of ε_1 and ε_2 to zero. Additionally, V_{pv} converges also to V_{pvref}. Moreover. The nonlinear controller of PWM is provided by Eq. (31).

3.2. Inverter Grid Side Control

For controlling the inverter grid side, it is a must to regulate the external loop and the internals loops. In this paper, the regulation of the three loops will be realized by the backstepping technique [20]. To control the V_{dc} of the external loop, let's insure the regulation tracking objective, firstly, let's specify the error:

$$\varepsilon_3 = V_{dcref}^2 - V_{dc}^2 \tag{32}$$

Next, differentiating the Eq. (32) and replacing Eq. (15) by its value, we get:

$$\dot{\varepsilon}_3 = \dot{V}_{dcref}^2 - \frac{2}{C_{dc}}\left(-\frac{3}{2}v_{dg}i_{dg}^* + P_{out}\right) \tag{33}$$

The purpose of the backstepping control method in this phase is to make the error ε_3 converge to zero. So in order to accomplish this condition, the i_{dg} is selected to be the virtual control variable in Eq. (33). The Lyapunov function is represented as:

$$V_3 = \frac{1}{2}\varepsilon_3^2 \tag{34}$$

Differentiating the Eq. (34), and replacing Eq. (33) in this equation, we obtain:

$$\dot{V}_3 = \varepsilon_3\left(\dot{V}_{dcref}^2 - \frac{2}{C_{dc}}\left(-\frac{3}{2}v_{dg}i_{dg}^* + P_{out}\right)\right) \tag{35}$$

Eq. (35) turn into:

$$\dot{V}_3 = \varepsilon_3\left(\dot{V}_{dcref}^2 - \frac{2}{C_{dc}}\left(-\frac{3}{2}v_{dg}i_{dg}^* + P_{out}\right) + \beta_3\varepsilon_3\right) \tag{36}$$

Where β_3 is a positive design parameter ($\beta_3 > 0$) In favor of controlling the error ε_3, the virtual control variable becomes:

$$i_{dg}^* = \frac{1}{v_{dg}}\left(\frac{2}{3}P_{out} - \frac{C_{dc}}{3}\left(\dot{V}_{dcref}^2 + \beta_3\varepsilon_3\right)\right) \tag{37}$$

Then, the derivative V_3 of Lyapunov function is definitely negative. From Eq. (37), it is clear that to maintain the control of active power P_a, the virtual control should be regulated. Consequently, by reason of controlling P_a and Q, the errors ε_4 and ε_5 concerning the desired variables i_{dg} and i_{qg} of the internals loops are defined as:

$$\varepsilon_4 = i_{dg}^* - i_{dg} \tag{38}$$

$$\varepsilon_5 = i_{qg}^* - i_{qg} \tag{39}$$

The ε_4 and ε_5 should converge to zero, to the benefit of controlling the P_a and Q respectively. Therefore, the dynamical error of Eq. (33) can be identified as:

$$\dot{\varepsilon}_3 = \dot{V}_{dcref}^2 + \frac{3}{C_{dc}}v_{dg}\varepsilon_4 \tag{40}$$

Besides, the dynamical errors ε_4 and ε_5 can be indicated as:

$$\dot{\varepsilon}_4 = \frac{di_{dg}^*}{dt} - \left(-\lambda_1 i_{dg} + \lambda_2 i_{qg} + \lambda_3\left(v_{di} - v_{dg}\right)\right) \tag{41}$$

$$\dot{\varepsilon}_5 = \frac{di_{qg}^*}{dt} - \left(-\lambda_1 i_{qg} - \lambda_2 i_{dg} + \lambda_3 v_{qi}\right) \tag{42}$$

In order to provide the asymptotic stability of this phase and to make the errors ε_3, ε_4 and ε_5 converge to zero, a composite Lyapunov function V_4 is introduced and its derivative needs to be negative.

$$V_4 = \frac{1}{2}\left(\varepsilon_3^2 + \varepsilon_4^2 + \varepsilon_5^2\right) \tag{43}$$

V_4 is used to derive the control algorithm. For this purpose, the derivative of V_4 is calculated along with the Eq. (33), (41) and (42)

$$\dot{V}_4 = \varepsilon_3\dot{\varepsilon}_3 + \varepsilon_4\dot{\varepsilon}_4 + \varepsilon_5\dot{\varepsilon}_5 \tag{44}$$

The derivative of V_4 is definitively negative, and by replacing Eq. (40), (41) and (42) in Eq. (44) we get:

$$v_{di} = \frac{1}{\lambda_3}\left(\frac{di_{dg}^*}{dt} - \left(-\lambda_1 i_{dg} + \lambda_2 i_{qg} - \lambda_3 v_{dg}\right) + \frac{3}{C_{dc}}v_{dg}\varepsilon_3 + \beta_4\varepsilon_4\right) \tag{45}$$

$$v_{qi} = \frac{1}{\lambda_3}\left(\frac{di_{qg}^*}{dt} - \left(-\lambda_1 i_{qg} - \lambda_2 i_{dg}\right) + \beta_5\varepsilon_5\right) \tag{46}$$

The derivative of Lyapunov function V_4 is definitely negative

Where β_4 and β_5 are positive design parameters ($\beta_4 >0$ and $\beta_5 >0$).

The nonlinear control of our inverter is provided by Eq. (37), (45) and (46).

4. Simulation Results

The simulation of PV system presented in Fig. 1 is developed in Matlab/Simulink environment. The PV system and the BSC parameters are marked in Table 1. In this simulation, the temperature is fixed at 25°C and the irradiation G profile is given in Fig. 5. Fig. 6, presents the error signals ε_1, ε_2, ε_3, ε_4 and ε_5, it can be noticed from this figure that the signals of the five errors converge to zero during the variation of irradiation G at 0,7 and 2 seconds with low fluctuations. Which indicate that the Lyapunov functions ensure the asymptotic stability of the system.

Table 1. PV system and BSC specifications

PV System	Parameters	Values
PV array	Maximum power (P_{mpp})	123kW
	Number of Parallel panels (N_{pp})	41
	Number of Series panels (N_{ss})	15
DC-DC Boost converter	DC bus voltage (V_{dc})	800V
	Input capacitor (C_{pv})	2000µF
	Output capacitor (C_{dc})	2000µF
	Inductor (L)	120.10^{-5} H
	Switching frequency (f_{boost})	5kHz
Three phase Inverter	Switching frequency (f_{inv})	10kHz
Three phase Filter	Resistance (R_f)	0.01Ω
	Inductor (L_f)	3mH
Backstepping Controller	β_1	600
	β_2	9.10^8
	β_3	45.10^3
	β_4	9.10^6
	β_5	15.10^7

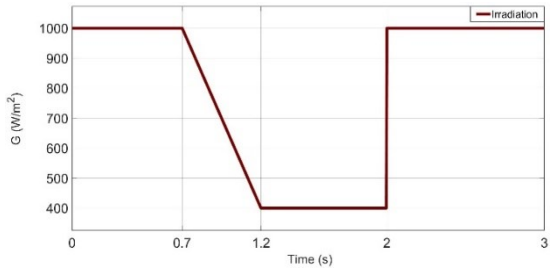

Fig. 5. Irradiation profile

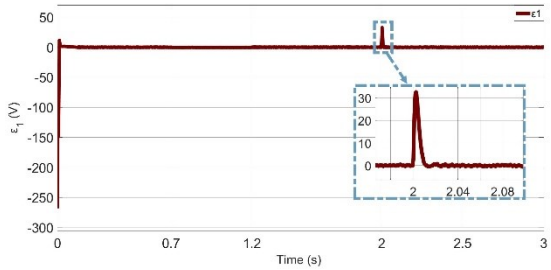

(a)

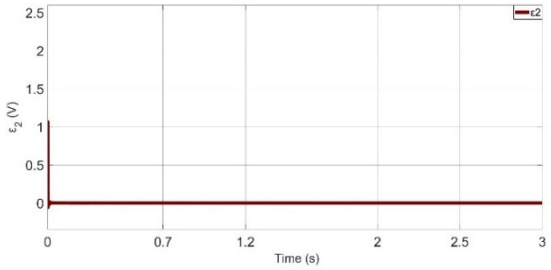

(b)

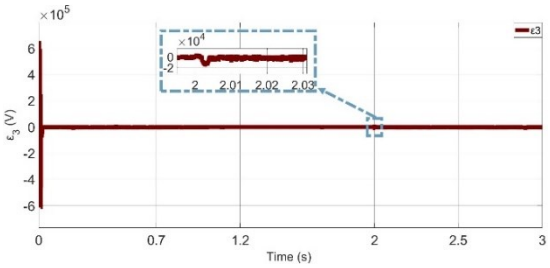

(c)

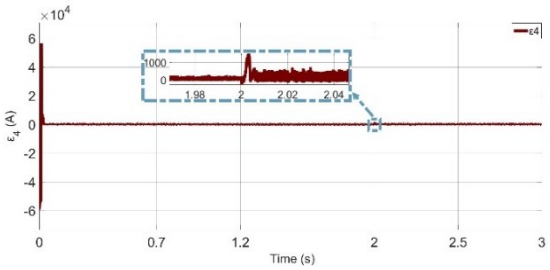

(d)

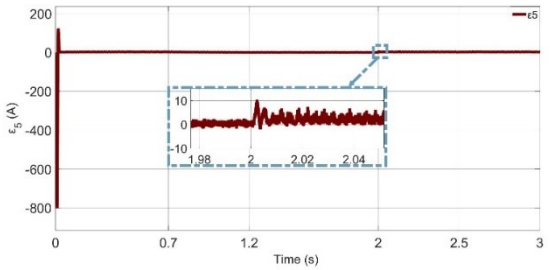

(e)

Fig. 6. (a) Error signal 1, (b) error signal 2, (c) error signal 3, (d) error signal 4, (e) error signal 5.

In Fig. 7 it is noticeable that the IC algorithm provides the exact V_{pvref} and the BSC tracks this reference successfully with less voltage variations.

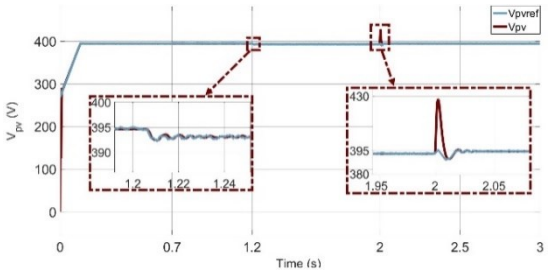

Fig. 7. Tracking of Vpv under irradiation variation

For the sake of verifying the performance of the BSC, a comparison is made between the MPPT of this controller and the classic IC MPPT during the irradiation profile variation, which is indicated in Fig. 8. From this latter, it can be noted that the IC-BSC provides the exact power value (123 kW) at the steady state with less oscillations. Moreover, this MPPT can reach the MPP value rapidly which is very clear at the transient state (from 400 to 1000W/m^2). Contrary to the IC MPPT that reaches the MPP with a lower convergence speed that leads to a marked delay. In addition, this classic MPPT

creates high oscillations at the steady state which is remarkable in the figure.

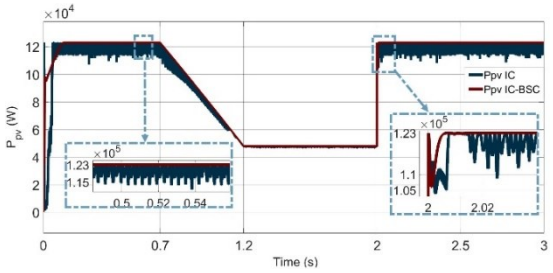

Fig. 8. Tracking the Ppv power of the PV array under irradiation variation with IC-BSC and IC MPPTs.

In purpose of confirming the validity of the BSC in inverter grid side, a comparative simulation study is made between this controller and the classic PI controller. The BSC provides a speedily feedbacks better than the classic PI controller, as it showed in Fig. 9 and Fig. 10. In the light of irradiation variation, it can be remarked in Fig. 9 that the BSC can reach the V_{dcref} value in a minimal response time "24ms", at the transient state from 0 to 1000W/m^2. Moreover, when the irradiation G changes from 400 to 1000W/m^2, the BSC attains the "800V" in 7ms. Not only this but this controller provides also a voltage signal with negligible fluctuations. Contrasted with the PI controller, that reaches the V_{dcref} value in a very long response time at is clear in the figure. Furthermore, this classic controller has also a major drawback which is the high fluctuations especially at the steady state. By the same token, the BSC attains the desired power value "123kW" in 0.03s, which is a short time response, as opposed to the PI controller that can arrive at the desired value in 0.07s as shown in Fig. 10 at the beginning of irradiation variation (from 0 to 1000W/m^2). Regarding the transient state (from 400 to 1000W/m^2), the BSC attains the desired value rapidly in 8ms with less oscillations, on the contrary the PI controller takes 16ms to reach the P_a value which is a very big delay. in addition, this controller provides major oscillations that are obvious in the figure. The classic PI controller also demonstrates that it has a remarkable delay and higher oscillations in comparison with our BSC that can track Q_{ref} speedily as improved in Fig. 11.

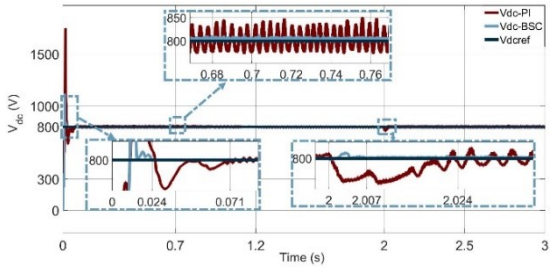

Fig. 9. Tracking the Vdc bus voltage under irradiation variation with BSC and PI controller.

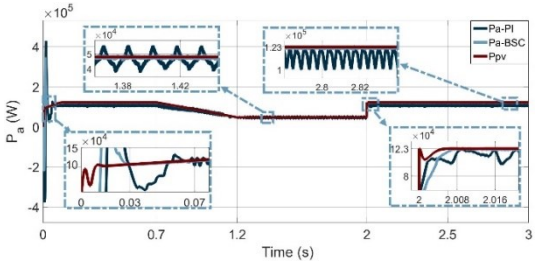

Fig. 10. Tracking the active power Pa under irradiation variation with BSC and PI controller.

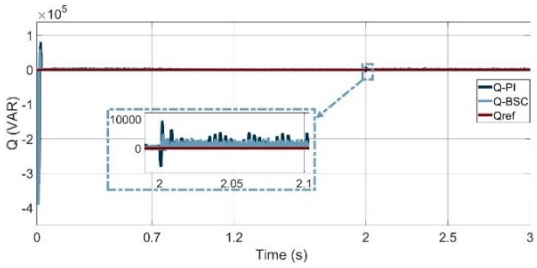

Fig. 11. Tracking the reactive power Q under irradiation variation with BSC and PI controller.

The Fig. 12 depicts the currents i_{gabc} injected into the grid, which they have a sinusoidal shape and their amplitudes follow rapidly the variation of irradiation G well. Furthermore, Fig. 13 shows that the grid voltage is in phase with the current which it is well balanced. Unlike the PI controller that shows in Fig. 14 big fluctuations concerning the current injected into the grid, even this latter is in phase with the grid voltage, but it still not performing better as the BSC. Accordingly, in the final analysis, the BSC provides very good performances with fewer fluctuations and without any remarkable delay at the MPPT level and the inverter grid level, in contrast to the IC MPPT and the PI controller, that they pose many drawbacks.

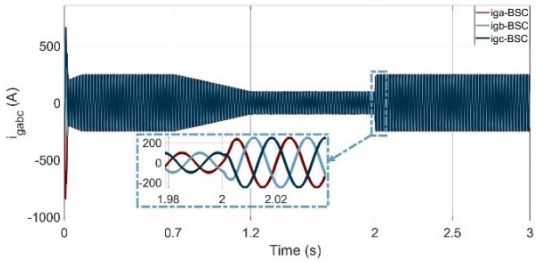

Fig. 12. Three phase currents of BSC injected into the grid.

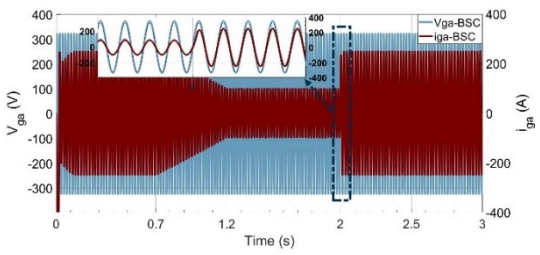

Fig. 13. Synchronization of the injected grid current with voltage Vga of BSC.

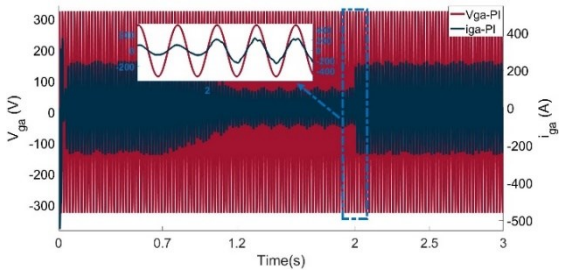

Fig. 14. Synchronization of the injected grid current with voltage Vga of PI controller

5. Conclusion

The essential objective of the current study was to apply a nonlinear backstepping controller for a PV system under the variation of irradiations. In the sake of checking the robustness and the effectiveness of the BSC, two comparisons are made, the first one was between the IC-BSC and the IC MPPT at MPPT level. While, the second was between the BSC and the PI controller at the inverter grid level. Based on the simulation results, all the five signal errors converge to zero, which strongly indicate that the Lyapunov functions ensured the asymptotic stability of the PV system. Additionally, the BSC tracks the V_{pvref} well with less voltage variation for the purpose that the IC algorithm provides the exact V_{pvref} voltage. Besides, the BSC produced a very satisfying response in terms of providing a P_{pv} power without any fluctuations differing from the IC MPPT. Further, the BSC offered a very satisfying achievement in terms of providing the exact maximum active power "123KW" with less fluctuations and without any marked delay as opposed to the PI controller which had a very big delay and major fluctuations. In the same way, the BSC also shown very good responses in terms of maintaining the V_{dcref} at "800V" value, and keeping up the reactive power at zero value under different operating conditions. As demonstrated above, the proposed controller provides an excellent performance with less fluctuations and without any important delay, which in reality prove the validity of this controller.

Acknowledgements

The authors would like to thank the Laboratory of Electronics, Instrumentation and Energy (LEIE), Chouaib Doukkali University, for providing the necessary facilities to conduct this research.

Author Contributions

O. Echab. was responsible for the conceptualization, validation, resources, data curation, software development, and project administration. N. Ech-Cherki, A. Obbadi , Y. Errami, S. Sahnoun and M. Aoutoul. jointly contributed to the methodology, formal analysis, investigation, original draft preparation, review and editing, visualization, supervision, and funding acquisition. All authors have read and agreed to the published version of the manuscript.

Conflict of Interest

The authors declare that there is no conflict of interest regarding the publication of this paper.

References

[1] I. Colak, R. Bayindir, and S. Sagiroglu, "The effects of the smart grid system on the national grids," 2020 8th International Conference on Smart Grid (icSmartGrid), Paris, France, pp. 122–126, 2020. doi: 10.1109/icSmartGrid49881.2020.9144891.

[2] C. Aoughlis, A. Belkaid, M. A. Kacimi, I. Colak, and O. Guenounou, "New dynamic and self-adaptive incremental conductance algorithm for standalone PV system," 2022 11th International Conference on Renewable Energy Research and Application (ICRERA), Istanbul, Turkey, pp. 268–273, 2022. doi: 10.1109/ICRERA55966.2022.9922758.

[3] N. K. Kasim, H. H. Hussain, and A. N. Abed, "Performance analysis of grid-connected CIGS PV solar system and comparison with PVsyst simulation program," International Journal of Smart Grid, vol. 3, no. 4, Dec. 2019. doi: 10.20508/ijsmartgrid.v3i4.5.

[4] B. K. Oubbati, M. Boutoubat, A. Rabhi, and M. Belkheiri, "Experiential integral backstepping sliding mode controller to achieve the maximum power point of a PV system," Control Engineering Practice, vol. 102, Sep. 2020. doi: 10.1016/j.conengprac.2020.104570.

[5] M. Mao, L. Cui, Q. Zhang, K. Guo, L. Zhou, and H. Huang, "Classification and summarization of solar photovoltaic MPPT techniques: A review based on traditional and intelligent control strategies," Energy Reports, vol. 6, pp. 1312–1327, Nov. 2020. doi: 10.1016/j.egyr.2020.05.013.

[6] M. Lawan, A. Aboushady, and K. H. Ahmed, "Photovoltaic MPPT techniques comparative review," 2020 9th International Conference on Renewable Energy Research and Application (ICRERA), Glasgow, UK, pp. 344–351, 2020. doi: 10.1109/ICRERA49962.2020.9242855.

[7] R. Z. Caglaya, K. Kayisli, N. Zhakiyev, A. Harrouz, and I. Colak, "A review of hybrid renewable energy systems and MPPT methods," International Journal of Smart Grid, vol. 6, no. 3, Sep. 2022. doi: 10.20508/ijsmartgrid.v6i3.248.g243.

[8] C. S. Kumar and G. Mallesham, "A new hybrid boost converter with P & O MPPT for high gain enhancement of solar PV system," Materials Today: Proceedings, vol. 57, part 5, pp. 2262–2269, Jan. 2022. doi: 10.1016/j.matpr.2021.12.487.

[9] S. F. Jaber and A. M. Shakir, "Design and simulation of a boost-microinverter for optimized photovoltaic system performance," International Journal of Smart Grid, vol. 5, no. 2, June 2021. doi: 10.20508/ijsmartgrid.v5i2.189.g145.

[10] S. D. Al-Majidi, M. F. Abbod, and H. S. Al-Raweshidy, "A novel maximum power point tracking technique based on fuzzy logic for photovoltaic systems," International Journal of Hydrogen Energy, vol. 43, no. 31, pp. 14158–14171, Aug. 2018. doi: 10.1016/j.ijhydene.2018.06.002.

[11] V. Kumar and M. Singh, "Reactive power compensation using derated power generation mode of modified P&O algorithm in grid-interfaced PV system," Renewable Energy, vol. 178, pp. 108–117, Nov. 2021. doi: 10.1016/j.renene.2021.06.035.

[12] Z. El Idrissi, H. El Fadil, F. Z. Belhaj, A. Lassioui, K. Gaouzi, and I. Bentalhik, "Real-time implementation of adaptive nonlinear control of Buck-Boost DC-DC power converter with a continuous input current for fuel cell energy sources," IFAC-PapersOnLine, vol. 55, no. 12, pp. 420–425, 2022. doi: 10.1016/j.ifacol.2022.07.348.

[13] H. Naghmash, H. Armghan, I. Ahmad, A. Armghan, S. Khan, and M. Arsalan, "Backstepping based non-linear control for maximum power point tracking in photovoltaic system," Solar Energy, vol. 159, pp. 134–141, Jan. 2018. doi: 10.1016/j.solener.2017.10.062.

[14] T. K. Roy and M. A. Mahmud, "A robust nonlinear backstepping control scheme for hybrid AC/DC microgrids to improve dynamic stability against external disturbances," Cleaner Energy Systems, vol. 3, Dec. 2022. doi: 10.1016/j.cles.2022.100044.

[15] I. Nassar-Eddine, A. Obbadi, Y. Errami, A. El Fajri, and M. Agunaou, "Parameter estimation of photovoltaic modules using iterative method and the Lambert W function: A comparative study," Energy Conversion and Management, vol. 119, pp. 37–48, July 2016. doi: 10.1016/j.enconman.2016.04.030.

[16] I. Ait Ayad, E. Elwarraki, and M. Baghdadi, "Intelligent perturb and observe based MPPT approach using multilevel DC-DC converter to improve PV production system," Journal of Electrical and Computer Engineering, vol. 2021, article ID 6673022, pp. 1–13, Feb. 2021. doi: 10.1155/2021/6673022.

[17] R. D. Middlebrook and S. Cuk, "A general unified approach to modelling switching converter power stages," International Journal of Electronics, vol. 42, pp. 521–550, Jan. 1977. doi: 10.1080/00207217708900678.

[18] A. Sangwongwanich, A. Abdelhakim, Y. Yang, and K. Zhou, "Control of single-phase and three-phase DC/AC converters," in *Control of Power Electronic Converters and Systems*, pp. 153–173, Academic Press, 2018.

[19] A. F. Alsulami and S. M. S. Al Arefi, "Fraction open circuit and fractional short circuit based incremental conductance maximum power point tracking controller," 2021 10th International Conference on Renewable Energy Research and Application (ICRERA), Istanbul, Turkey, pp. 184–189, 2021. doi: 10.1109/ICRERA52334.2021.9598557.

[20] Y. El Mourabit, A. Derouich, A. Allouhi, A. El Ghzizal, N. El Ouanjli, and O. Zamzoum, "Nonlinear backstepping control for PMSG wind turbine used on the real wind profile of the Dakhla-Morocco city," International Transactions on Electrical Energy Systems, vol. 30, no. 4, Apr. 2020.

.